Cellular tagging for MRI: Budde and Frank review the various methods used for magnetic labeling of cells for tracking with MRI and the potential for such methods in clinical applications. . . . . ***Page 171***

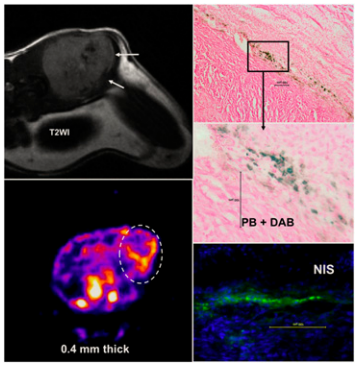

Changing paradigms in ischemic heart disease: Neglia and L'Abbate provide perspective on current understanding and emerging approaches in assessment of coronary artery and ischemic heart disease, including PET techniques for diagnosis and monitoring of progression and treatment. . . . . ***Page 175***

PET and insulin effects: Roy and colleagues evaluate a standardized protocol of intravenous insulin administration in reducing glycemia in diabetic cancer patients undergoing ^{18}F-FDG PET and assess tracer biodistribution and clinical effects. . . . . ***Page 178***

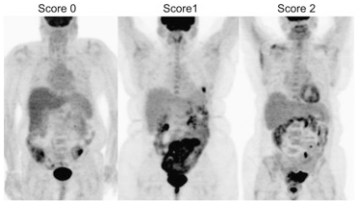

^{131}I SPECT/CT in thyroid cancer: Spanu and colleagues compare the results of SPECT and integrated low-dose CT with those from planar imaging in detecting residual disease and metastases in patients with differentiated thyroid cancer. . . . . ***Page 184***

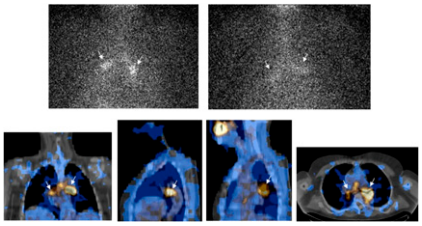

Tracers for Alzheimer's detection: Tolboom and colleagues investigate ^{11}C-PiB and ^{18}F-FDDNP as PET tracers for imaging and differentiation of pathology in patients with Alzheimer's disease and patients with mild cognitive impairment. . . . . ***Page 191***

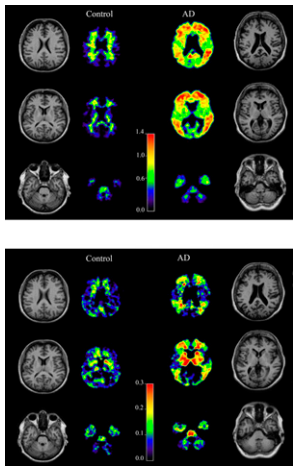

PiB binding to white matter: Fodero-Tavoletti and colleagues characterize the nature and kinetics of Pittsburgh Compound B binding in white matter in the brain and discuss the implications for ^{11}C-PiB PET imaging in neurodegenerative disease. . . . . ***Page 198***

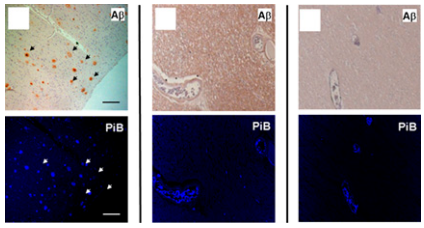

Automatic LV segmentation in MPS: Soneson and colleagues validate a novel method for automatic segmentation of left ventricular mass in myocardial perfusion SPECT, with advantages in estimating the perfusion defect size as a percentage of the left ventricle. . . . . ***Page 205***

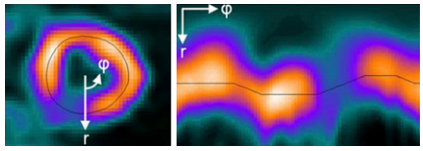

Predicting cardiac death: Tio and colleagues compare the prognostic value of conventional left ventricular ejection fraction with that of myocardial perfusion reserve as assessed by PET in patients with ischemic heart disease. . . . . ***Page 214***

β-Receptor blockade in cardiomyopathy: Naya and colleagues use ^{11}C-CGP12177 PET to measure myocardial β-adrenergic receptor density as a potential predictor of improvement in cardiac function during β-blocker carvedilol treatment for idiopathic dilated cardiomyopathy. . . . . ***Page 220***

Interactive multimodality stress testing: Walimbe and colleagues describe a new multimodality stress test for accurate correlation of complementary functional and perfusion information from real-time 3D echocardiography and SPECT. . . . . ***Page 226***

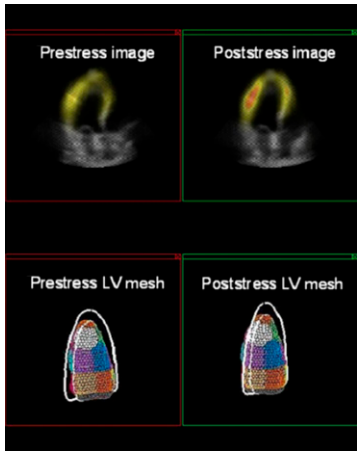

PET/CT in inflammatory breast cancer: Carkaci and colleagues report on results from a retrospective study evaluating ^{18}F-FDG PET/CT in the initial staging of inflammatory breast cancer. . . . . ***Page 231***

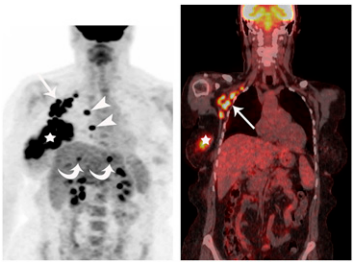

Biomarkers of response: Zhao and colleagues provide an educational overview of the current status of quantitative imaging as a surrogate biomarker for assessment of tumor response to therapy, using non–small cell lung cancer as an example. . . . . ***Page 239***

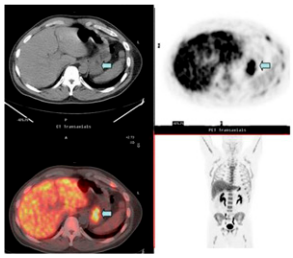

Compartmental model for ^{64}Cu-DOTA-RGD: Ferl and colleagues present a compartmental model to describe time–activity curves after intravenous injection of radiolabeled arginine-glycine-aspartate peptides for PET imaging in cancer studies. . . . . ***Page 250***

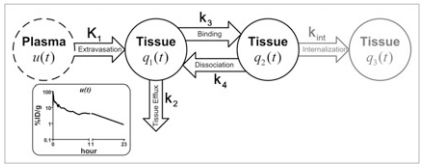

Delayed enhancement in cardiac PET/CT: Holz and colleagues determine the feasibility of delayed CT enhancement in the PET/CT environment and compare the results with PET-defined rest perfusion of measurement of infarct size in a swine model. . . . . ***Page 259***

PET and intestinal ulceration: Yamato and colleagues report on preclinical investigations of the utility of ^{18}F-FDG PET for noninvasive monitoring of indomethacin-induced small-intestine ulceration. . . . . ***Page 266***

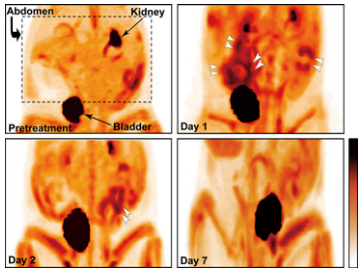

EGFR-specific affibody molecules: Tolmachev and colleagues report on a novel epidermal growth factor receptor–targeting protein for radionuclide imaging and on research to determine a suitable tracer format and optimal labeling. . . . . ***Page 274***

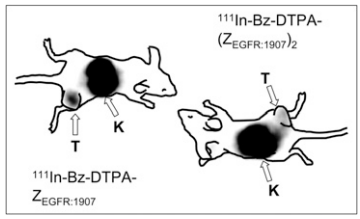

Serotonin receptor binding and canine anxiety: Vermeire and colleagues use ^{123}I-5I-R91150 SPECT to evaluate the involvement of the brain 5-HT2A receptor in dogs with severe anxiety disorder. . . . . ***Page 284***

D-^{18}F-FMT monitoring of radiation response: Murayama and colleagues compare the potential of a promising agent for PET imaging of early tumor response to radiation therapy with that of other conventional ligands in a mouse model. . . . . ***Page 290***

Improving anti-CD45 mAb RIT: Kletting and colleagues report on the development of a physiologically based pharmacokinetic model to determine individually optimized preloads for radioimmunotherapy with this radiolabeled monoclonal antibody. . . . . ***Page 296***

Radiation dosimetry of ^{11}C-PD153035: Liu and colleagues characterize the biodistribution and radiation-absorbed dose of this epidermal growth factor receptor radioligand in whole-body PET studies of healthy volunteers and discuss the radiation safety advantages of its use in serial studies. . . . . ***Page 303***

Radiation dosimetry of β-amyloid tracers: O'Keefe and colleagues calculate and compare the effective doses of ^{11}C-PiB and ^{18}F-BAY94-9172, a new ^{18}F-labeled ligand, and assess the suitability of their respective dosimetries for clinical and research applications. . . . . ***Page 309***

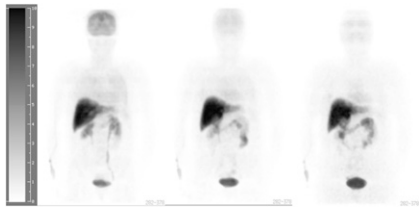

Patient morphology and dosimetric calculation: Divoli and colleagues investigate the differences between patient-specific dosimetric results obtained using the Monte Carlo method and those obtained using S factors calculated on standard models. . . . . ***Page 316***

ON THE COVER

In a pig model of chronic myocardial infarction, infarct size can be measured by cardiac PET/CT and delayed CT enhancement. A low-dose, prospectively gated acquisition obtained as early as 10 min after contrast injection achieves measurements comparable to those of rest perfusion PET. The colored areas in these polar maps represent global defects after applying a threshold of 3.5 SDs above the mean of remote myocardium for CT.

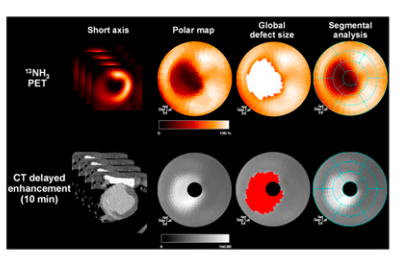

See page 263.